APL Energy

RESEARCH ARTICLE | JULY 21 2025

Ionic accumulation and depletion space-charge zones at metal halide perovskite contacts from device numerical simulations

Special Collection: Novel Simulation Approaches of Perovskite Optoelectronic Devices and Materials

Germà Garcia-Belmonte ; Osbel Almora

APL Energy 3, 036103 (2025)
https://doi.org/10.1063/5.0267693

Ionic accumulation and depletion space-charge zones at metal halide perovskite contacts from device numerical simulations

Cite as: APL Energy 3, 036103 (2025); doi: 10.1063/5.0267693
Submitted: 25 February 2025 • Accepted: 2 July 2025 •
Published Online: 21 July 2025

Germà Garcia-Belmonte[1,a)] and Osbel Almora[2]

AFFILIATIONS

[1] Institute of Advanced Materials, Universitat Jaume I, 12071 Castelló, Spain
[2] Department of Electronic, Electric and Automatic Engineering, Universitat Rovira i Virgili, 43007 Tarragona, Spain

Note: This paper is part of the Special Topic on Novel Simulation Approaches of Perovskite Optoelectronic Devices and Materials.
[a)] **Author to whom correspondence should be addressed:** garciag@uji.es

ABSTRACT

The inherent ion migration in metal halide perovskite is known to induce instabilities into the operation of solar cells and radiation detectors based on these compounds. For instance, dark current slow drift with time has been identified among the major drawbacks for X- and γ-ray detectors to satisfy industrial requirements. Conversion efficiency in photovoltaic devices usually exhibits significant reduction upon continuous illumination. In both cases, the formation of ion-related space-charge zones at the vicinity of the electrode interfaces (electrode polarization upon biasing) is believed to play a major role in the degradation of the device functioning. By using 1D numerical simulation tools, two dissimilar charged structures are identified after voltage application in the steady state: a narrow and huge ion accumulation near one electrode compensated by a spatially extended depletion zone at the opposite one. Ion accumulation zone width correlates with the ionic Debye length for ion concentration below a certain limit. In addition, more extended ion depletion zones follow the dependencies usually encountered in semiconductor contacts inversely proportional to the square root of ion concentration and proportional to the square root of voltage. Deviations from classical models are also discussed in relation to the theoretical assumptions.

I. INTRODUCTION

A decade ago, in the mid-2010s, anomalous current–voltage hysteresis was identified[1,2] in metal halide perovskite-based solar cells (PSCs) alerting on the deleterious role that some intrinsic physical mechanisms play in those compounds, which were rarely encountered in other semiconductor photovoltaic devices.[3] At that moment, the appearance of hysteretic effects fostered an intense debate about their origin and repercussion on the perovskite solar cell performance and casted doubts about the applicability of that new and promising technology.[4,5] Among other competing explanations such as ferroelectricity[6] and slow electronic carrier trapping,[7] the hypothesis of ion migration gained great acceptance as the cause of hysteresis and other slow (low-frequency) effects.[1,5,8] In fact, compounds with similar crystalline structure as metal oxide perovskites[9] were well-known and exploited because of their high ionic conductivity. It was envisaged that perovskite-based devices, hence exhibiting mixed electronic–ionic conduction, could present the kind of mechanisms usually encountered in purely ionic conductors. Consequently, we proposed in 2015 that, upon electrical poling in the dark, electrode polarization occurs as a consequence of the interfacial accumulation of moving ions at the outer contacts.[10] This last mechanism explained the perovskite layer's excess (low-frequency) capacitance and was correlated with the observed current–voltage hysteresis. Further evidence supporting this hypothesis has been reported under dark conditions,[11] while mixed results have been observed under illumination conditions,[12] where the presence of additional photogenerated charge carriers complicates the charge density profile as well as the resistive and capacitive responses.[13]

Several studies have tried to probe the existence and principal features of the ionic space-charge structures resulting upon electrode polarization in PSC operation. Using Kelvin probe force microscopy,

a redistribution of local surface potential was detected by Yuan *et al.*, who stated to be caused by ion migration.[14] Furthermore, the formation of interfacial charge zones in the negative electrode of width <50 nm was observed by Weber *et al.* in ~500 nm-thick perovskite layers under a voltage-step stimulus[15] that screened most of the internal electrical field. That charging was compensated by a more extended, exponential potential decay in the opposite electrode.

More recently, a highly anisotropic polarization has been observed by Wang *et al.* in all-inorganic perovskites.[16] There, a strong built-in electric field within a submicrometer length near the cathode was reported exhibiting an exponential decay into the perovskite layer bulk. Other studies have highlighted a major influence of the interface chemistry and polarity on the ion adsorbing properties.[17] Alternative experimental approaches use electro-absorption measurements that allow the electric field within the active layer to be tracked as a function of frequency or time.[18] All these approaches infer a significant internal field screening as a consequence of the dynamics of moving ions affecting device stability and long-term performance.[19,20]

Purely electric measurements have also suggested the formation of interfacial ionic space-charge zones. For instance, Kim *et al.* monitored the voltage change in galvanostatic experiments and suggested ionically determined equilibrium space-charge potentials in methylammonium lead iodide contacted by Al_2O_3 and TiO_2.[21] Moreover, a pulsed measurement technique has been developed by Hill *et al.* for characterizing the electrostatic potential energy drop across perovskite layers in functioning devices.[22] This technique allows measuring the energy-band alignment at extracting contacts influenced by the mobile ion interfacial pileup. Furthermore, low-frequency capacitive analysis[10,23,24] and charging experiments[25,26] have been correlated with the occurrence of interfacial ionic accumulation and the built-up of ionic space-charge structures. However, despite all the information gathered through direct experimental tools, a clear picture of the main features ionic space-charge structures exhibit is still missing.

Alternatively, device simulation methods have been exploited to gain further insight into the determinant effect of ion movement and accumulation under the application of electrical bias or light. Nowadays, 1D drift-diffusion numerical approaches are widely used to complement experimental analyses.[27] They have been applied both to perovskite solar cells[18,28] and X-ray perovskite detectors.[20,29,30]

One interesting outcome of single moving-ion simulations was observed by Richardson *et al.*, who found distinct accumulation and depletion space-charge zones depending on the ion charge sign at respective contacts.[31] Although the authors did not deepen on the distinct space-charge zone characteristics. These dissimilar charged structures (a high-density, spatially confined ion accumulation near one electrode compensated by a spatially extended depletion zone at the opposite one) have been corroborated in recent years.[20,24,29,30] However, there is a lack of exhaustive analysis of the referred ionic distributions upon applied voltage change and, more importantly, how are they connected to the classical polarization mechanisms largely studied for solid and liquid electrolytes.

Ionic space-charge zones and ion dynamics greatly influence device operation by modifying electronic injection barriers, explaining current instabilities (such as hysteresis and current drift upon bias), and potentially contributing to degradation paths and reduced operation performance (through field screening).[32] Therefore, this calls for new theoretical insights, supported by numerical simulation analysis, to deepen our knowledge about ionic space-charge built-up processes.

In this work, we carried out a set of 1D numerical simulations mimicking the structure and using typical material parameters of perovskite-based devices such as solar cells and X- and γ-ray detectors with a single species of mobile ions. Ionic space-charge zones are identified in the vicinity of the outer electrodes and their functional dependencies on equilibrium ion concentration and electrostatic potential are analyzed under steady-state conditions after application of a step voltage perturbation under dark conditions. As noted previously, dissimilar distributions occur depending on the ion charge sign and electrode polarization. The widths of accumulation and depletion zones as derived from the simulation are confronted with classical theoretical models. It is inferred that ion accumulation zones correlate with the ionic Debye length for ion concentration below a certain limit. In addition, more extended ion depletion zones follow the dependences usually encountered in semiconductor contacts but with moving ions playing the role of electronic charge carriers.

II. IONIC ELECTRODE POLARIZATION THEORETICAL APPROACHES

Classical analyses on polarization of electrolyte interfaces predict the formation of two main ionic structures under dark conditions related with the response of the interfacial double-layer: a narrow Helmholtz plane of molecular extension and an electrode-induced local charge imbalance within the wider ion diffuse layer.[33] Here, the Gouy–Chapman theory for the diffuse layer structure assumes Poisson equation and Boltzmann distribution in the mean field approach, while it neglects strong chemical interaction that may occur, for instance, between the perovskite layer and the selective transport contact materials. The theory is also valid for diluted electrolytes (neglecting statistical correlations) of moving ion in small concentrations.[34] The characteristic polarization width corresponds to the ionic Debye length as

$$\lambda_D = \sqrt{\frac{\varepsilon_0 \varepsilon_r k_B T}{Q^2 N_{ion}}}. \tag{1}$$

Here, T is the temperature; k_B is the Boltzmann constant; ε_r is the dielectric constant; ε_0 is the vacuum permittivity; and Q is the ion charge. N_{ion} accounts for the equilibrium ionic density throughout the bulk of the perovskite layer. In the specific case of PSCs, we proposed a decade ago that an ionic Debye length such as that of Eq. (1) could result from the electrode polarization, enabling low-frequency excess capacitance values.[10,25] Note that Eq. (1) implies $\lambda_D \propto N_{ion}^{-1/2}$ and it is voltage-independent.

While the Gouy–Chapman theory predicts similar distributions in the oppositely polarized electrode (ion depletion), a less explored structure has been proposed[35] mimicking that derived in the case of semiconductor contacts forming electronic depletion zones.[36] Here, the critical length corresponds to the depletion layer width as

$$\lambda_{dep} = \sqrt{\frac{2\varepsilon_0 \varepsilon_r V_{dep}}{QN_{ion}}}. \quad (2)$$

Here, V_{dep} accounts for the potential drop at the depletion layer (a portion of the external applied voltage). Note that the proposed structure in Eq. (2) is purely ionic in nature following the same dependence with the equilibrium ion concentration as that predicted by Eq. (1), i.e., $\lambda_{dep} \propto N_{ion}^{-1/2}$. However, contrary to Eq. (1), the ion depletion width also varies with the voltage drop as $\lambda_{dep} \propto V_{dep}^{1/2}$. It is worth recalling that purely electronic space-charge structures of the same kind (accumulation and depletion) develop in metal–semiconductor contacts.[37]

III. RESULTS AND DISCUSSION

The numerical simulations were conducted using an adapted code from MATLAB's Driftfusion framework,[27] incorporating both radiative and non-radiative recombination while adhering to four main assumptions. First, the perovskite bulk is initially assumed to be intrinsic, ensuring the total equilibrium concentrations of fixed and mobile ions remain balanced, meaning an equal number of cations and anions in our simulation or an effective balance near the intrinsic carrier concentration in experimental scenarios. Second, the interface regions between the perovskite and the contacts are unintentionally doped, favoring the formation of space-charge layers. Third, only one type of mobile ion is considered to significantly contribute to both the current and the redistribution of the charge density profile. Considering the prototypical family of compounds $MAPbX_3$, it is widely admitted that halide vacancies V_X^+ exhibit larger mobility values than those encountered for slower migrating defects as MA or Pb vacancies.[15,38,39] As a consequence, only one type of defect, i.e., V_X^+, is allowed to move within the temporal framework of the simulation. Finally, the built-in electric field is defined solely by the difference in work functions between the two metal contacts.

The parameters used in the following simulations are consistent with those in our previous experimental and theoretical work.[29] A summary can be found in Table S1 (supplementary material). The device structure includes metallic electrodes, electron and hole selective layers, and the perovskite absorber. At each interface of the perovskite layer, a numerically convenient 1 nm-thick interlayer was also included. The perovskite properties relate to $MAPbI_3$. The diffusion coefficients are a function of mobility according to Einstein's relation.[27] The stabilization time for convergence of steady-state solutions was set to 10 ks.

Here, the formation of steady-state, ionic space-charge zones is investigated after application of an external voltage, which is maintained until complete ion rearrangement under long-term biasing conditions. In the steady state, current saturates because of the ionic modulation of the electronic injection properties at the contacts, closely related to the ionic space-charges built up at the outer electrodes.[38] Dynamics of contact charging/discharging were addressed in previous studies, exhibiting for wider layer thicknesses long current transients in the time scale of ~10^4 s.[20,29]

By examining Fig. 1, one can infer that the mobile ion concentration profile (in the steady state) exhibits distributions resembling those previously discussed: a narrow and huge ion accumulation near the right, negatively polarized electrode compensated by a spatially extended depletion zone at the left, positively polarized one. Here, normalized curves with respect to the perovskite layer thickness L are represented for different values of N_{ion} within the range usually encountered in the literature.[24,40] As expected, both space-charge zones shrink as N_{ion} increases.

An operational definition for the accumulation space-charge-zone width w_{acc} is proposed with respect to the maximum concentration of mobile ions $N_{\max}$, attained toward the right electrode in the example of Fig. 1 (also see Fig. S1). In this case, w_{acc} is defined to match the position where the percentage of concentration is taken from the ratio $N_{ion}/N_{\max}$. Figure 1 also shows the illustrative example where the value for w_{acc} corresponds to the distances from the electrode (to the right) to the positions (to the left) where the concentration of mobile ions is increased an amount that matches 0.5% of $N_{\max}$. Notably, this definition is particularly convenient for estimating w_{acc}, such as in the case $w_{acc}(N_{\max}, 0.5\%)$ approaches the Debye length (λ_D) defined in Eq. (1) (also see Fig. S1 and below). However, depending on $N_{\max}$ makes the analysis sensitive to divergence of solutions, which can create unrealistically high values for $N_{\max}$ toward the interfaces.

For the estimation of the depletion space-charge width w_{dep}, we adopt a different approach using the ionic concentration in the

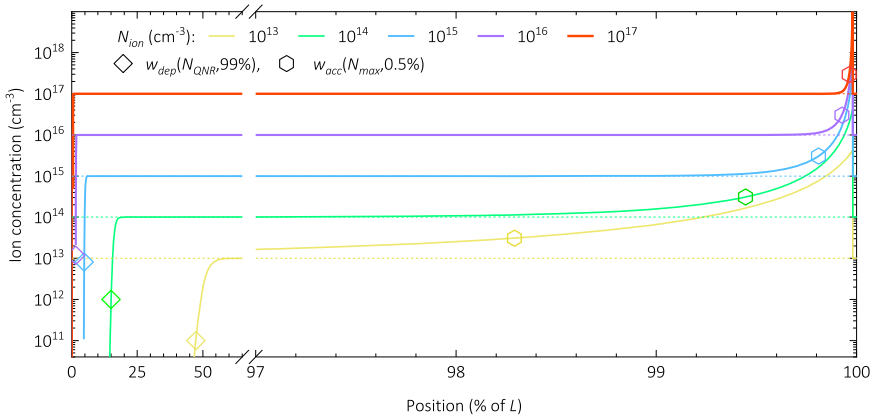

FIG. 1. Mobile ion concentration profile as resulting from the application of a step voltage perturbation after reaching the steady-state conditions, for different equilibrium values of N_{ion}. Perovskite layer thickness is $L = 100$ μm, and applied voltage is $V = 1$ V. Accumulation width $w_{acc}(N_{\max}, 0.5\%)$ and depletion width $w_{dep}(N_{QNR}, 99\%)$ are marked.

quasi-neutral region (QNR, flat ion concentration in the central part of the perovskite layer bulk) N_{QNR} as a reference. Here, w_{dep} represents the region with the lowest concentration of mobile ions. In this region approaching the left electrode, the charge is primarily determined by the oppositely charged (fixed) ions. By definition, w_{dep} is determined here as the position where the relative concentration decrease is quantified by the ratio abs$(N_{ion}\text{-}N_{QNR})/N_{QNR}$. This is illustrated on the left part of Fig. 1, where an example is provided. The values of $w_{dep}(N_{QNR}, 99\%)$ correspond to the distances from the electrode (on the left) to the positions (on the right) where the concentration of mobile ions decreases to 99.9% of its value in the quasi-neutral region (QNR).

It is also interesting to explore the profile of the steady-state electrostatic potential drop reached after external potential application. Due to the dissimilar space-charge zones built up at the positively and negatively polarized electrode, one would also expect asymmetries regarding the internal potential distribution. It is shown in Fig. 2 that the potential largely drops within the depletion zone, while the contribution to the potential variation at the accumulation region (right side) becomes relatively small in comparison with the left side. Therefore, one can safely assume as a first approximation that $V_{dep} \approx V$, while $V_{acc} \approx 0$, with V being the external applied voltage.

Our main objective is to confront the ionic space-charge widths (both at the accumulation and depletion zones) with theoretical approaches previously introduced in Eqs. (1) and (2). Therefore, dependencies of w_{acc} and w_{dep}, as derived from the simulation, with the parameters N_{ion} and V should be explored. This is illustrated in Fig. 3. In Fig. 3(a), space-charge widths follow the dependence with the ion concentration as $\propto N_{ion}^{-1/2}$, both for the accumulation and depletion zone. A deviation is encountered for both w_{dep} and w_{acc} in the case of $N_{ion} > 10^{16}$ cm^{-3} that under- and over-estimates the expected trend, respectively. Possible explanations are presented in the following. Theoretical approaches of Debye length λ_D and depletion width λ_{dep} in Eqs. (1) and (2) are also depicted for comparison.

To explore the voltage-dependence of the characteristic lengths, we select $N_{ion} = 10^{13}$ cm^{-3}, but similar trends are expected for $N_{ion} > 10^{13}$ cm^{-3}. By examining Fig. 3(b), one can infer that w_{dep} effectively obeys the expected voltage-dependence as $w_{dep} \propto V^{1/2}$. Simulations of the depletion layer enlargement with

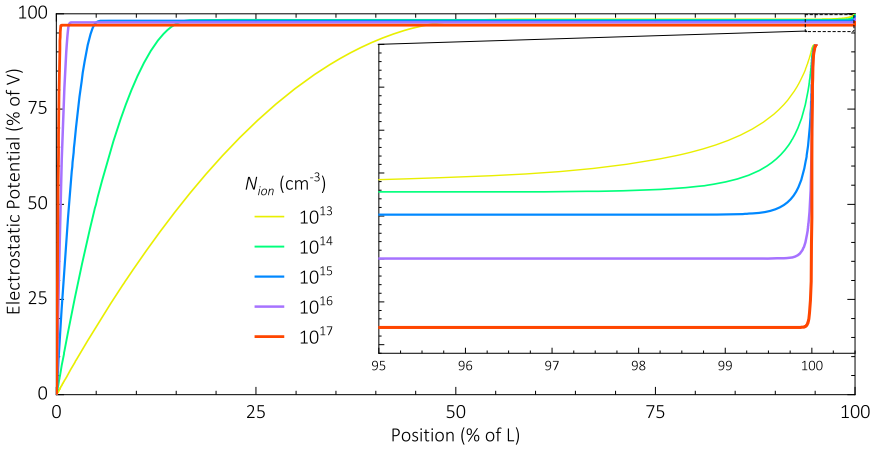

FIG. 2. Electrostatic potential profile after reaching the steady-state conditions, for different equilibrium values of N_{ion}. Perovskite layer thickness is $L = 100$ μm, and applied voltage is $V = 1$ V. A large potential drop is observed in the space-charge depletion zone (left side), while the accumulation zone (in the inset) contributes with a small portion.

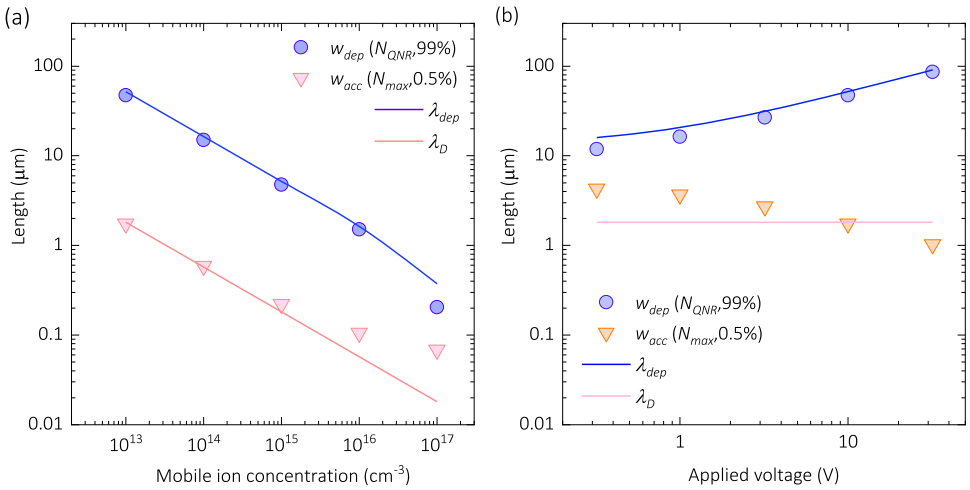

FIG. 3. Dependencies of $w_{acc}(N_{max}, 0.5\%)$ and $w_{dep}(N_{QNR}, 99\%)$ with (a) ion concentration N_{ion} and (b) applied voltage V. In panel (a), $V = 10$ V, and $N_{ion} = 10^{13}$ cm^{-3} in panel (b). λ_D and λ_{dep} are also plotted.

applied voltage are shown in the supplementary material (Fig. S2). The main deviation occurs when w_{acc} and λ_D are compared. Instead of a constant value, as derived from Eq. (1), w_{acc} exhibits a decrease by a factor of four, with λ_D as a sort of average value. In any case, its voltage-dependence is minor, as clearly observed in Fig. S2. We can envisage three possible explanations for this. (i) We have assumed $V_{dep} = V$ for the sake of simplicity, which strictly speaking implies $V_{acc} = 0$. However, by observing Fig. 2, one can see that the potential drop in the accumulation zone, although small, is not negligible. This would cause significant variations of λ_D when plotted as a function of V instead of V_{acc}. (ii) Derivation of accumulation zone, in the framework of the Gouy–Chapman theory, considers a semi-infinite structure with only one interface. However, our system model comprises a perovskite layer with two interfaces as contacts. Therefore, an analytical solution will be needed to complete a proper comparison with the simulation results. This explanation is also valid for deviations of the depletion width from the relation $\propto N_{ion}^{-1/2}$ at larger ion concentrations in Fig. 3(a). (iii) Other causes of deviation would be related to the appearance of statistical inter-ionic interactions at higher ion concentrations [Fig. 3(a)] or the influence of the electrostatic energy exceeding the thermal energy (one of the assumptions in deriving the Gouy–Chapman outcome) [Fig. 3(b)]. In addition, note that λ_{dep} is calculated using V_{dep} Eq. (2) which induces a deviation from the constant slope $\propto N_{ion}^{-1/2}$ for $N_{ion} > 10^{16}$ and low bias. In any case, we regard our analysis as a valid first approximation to the problem because it captures the basic dependencies $\propto N_{ion}^{-1/2}$ and $V^{1/2}$, in good accordance with the theoretical approaches, in a wide ion concentration interval.

One of the implications of our findings relates to the measurement of the capacitance variation with the applied voltage following the classical Mott–Schottky (MS) analysis, with the aim of estimating ion concentrations. As known, the voltage-modulation of the ionic charge in the space-charge regions gives rise to capacitances per unit area as $C_{dep} = \varepsilon_0\varepsilon_r/\lambda_{dep}$ and $C_D = \varepsilon_0\varepsilon_r/\lambda_D \exp(qV_{acc}/2k_BT)$, for depletion and accumulation zones, respectively. Note that C_D appears in series with the Helmholtz layer capacitance $C_H = \varepsilon_0\varepsilon_r/l$ (l being the separation of molecular length contacting the interface) in such a way that the inverse of total capacitance is $C_D^{-1} + C_H^{-1} + C_{dep}^{-1}$. Because $l \ll \lambda_D \ll \lambda_{dep}$, one should expect a total capacitance dominated by that of the depletion layer $C \approx C_{dep}$. Therefore, Eq. (2) suggests that, for samples whose perovskite thickness L is longer than λ_{dep}, a steady-state MS relation $C^{-2} \propto V$ should be measurable with a slope proportional to N_{ion}^{-1}.

Considering non-stationary MS data with high-frequency (~10 kHz) capacitance from our experiments of bias scan rate-dependent hysteresis in the capacitance-voltage curves in 2016, we initially suggested that mobile-ions were affected by the bias sweep, then actively modifying the space charge region widths.[36] These observations were consistent with the following experiments[41] such as those presented in Fig. 4(a). Subsequently, Fischer *et al.*[42] performed MS analyses after pre-biasing conditions. Their findings indicated that the reordering of migrating ions is strongly influenced by biasing voltage, time, and temperature and it could result in linear behaviors following the relationship $C^{-2} \propto V$. Under the assumptions of extremely thin and highly doped selective contacts, along with a perovskite layer containing two mobile ion species of opposite signs, this MS behavior was proposed to form a p–n junction within the perovskite, allowing for the estimation of effective N_{ion} values.

However, in the absence of corroborating evidence for the estimated N_{ion} values, as well as the number and polarity of the migrating ion species, it remains unclear whether thin film samples such as PSCs may have $\lambda_{dep} \geq L$ within the explored voltage range. This full depletion scenario raises doubts about whether the relatively high effective "doping densities" inferred from pre-biased MS experiments (typically in the order of 10^{17} cm^{-3})[41–43] truly represent mobile ions or reflect a more complex scenario of series-connected depletion layer capacitances including the doping levels in the selective layers, whose thicknesses may not be negligible in practical devices. In addition, the obtention of MS behavior from PSCs measured in typical voltage and temperature conditions is still difficult, even with pre-bias or combinations of slow and fast voltage scan rates. This could be due to $\lambda_{dep} \geq L$ conditions and/or inconvenient experimental values of ion mobility and concentration.

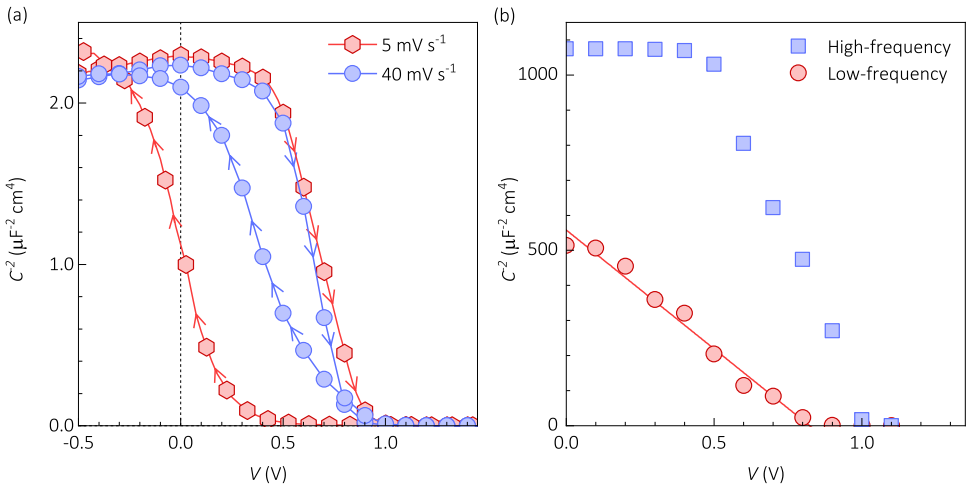

FIG. 4. Capacitance as a function of bias voltage MS representation showcasing the effects of (a) sweep scan rate and (b) frequency modulation in PSCs. The arrows in panel (a) indicate the direction of the bias scan sweep and the solid line in panel (b) highlights the MS behavior. Adapted with permission from O. Almora, Ph.D. thesis, Friedrich-Alexander Universität Erlangen-Nürnberg & Universitat Jaume I, 2020.[41]

In 2020,[41] we observed that while some PSCs did not exhibit MS behavior in high-frequency capacitance-voltage measurements, regardless of pre-bias or scan rate conditions, they did display clear MS behavior when analyzed using stationary low-frequency (<1 Hz) capacitance data. This is illustrated in Fig. 4(b). Based on these observations, we hypothesized that the low-frequency MS signal arises exclusively from the bias-dependent modulation of space charge region widths formed by mobile ions. In addition, we suggested that the accuracy of the estimated N_{ion} values would critically depend on the precision of the low-frequency capacitance values. In cases where no clear steady-state low-frequency saturation is observed in the capacitance Bode plots, these values should be extracted through appropriate equivalent circuit modeling to ensure reliability. Notably, although this work does not include capacitance simulations, the experimental data presented in Fig. 4 qualitatively support our previous discussion. These observations are also consistent with the more recent study by Diekmann *et al.*[24] who validated similar experimental findings through drift-diffusion simulations and charge extraction techniques, confirming the link between mobile-ion-induced space charge modulation and the observed low-frequency MS behavior.

IV. CONCLUSIONS

Here, 1D numerical simulations of perovskite-based devices such as solar cells and x- and γ-ray detectors have been performed. Simulation tools use typical material parameters and structures. Steady-state ionic space-charge zones are specifically addressed that build up in the vicinity of the electrode interfaces upon application of an external step bias (electrode polarization). Two dissimilar charged structures (a narrow and huge ion accumulation near one electrode compensated by a spatially extended depletion zone at the opposite one) result from the analysis under dark conditions. It is revealed that ion accumulation zones correlate with the ionic Debye length for ion concentration below a certain limit. In addition, more extended ion depletion zones follow the dependencies usually encountered in semiconductor contacts, but with moving ions playing the role of electronic charge carriers. Hence, both ionic space-charge regions behave as $\propto N_{ion}^{-1/2}$, while the depletion one also presents a voltage-dependence as $\propto V^{1/2}$. Deviations from these general trends are also discussed in relation to the theoretical assumptions. Implications of our findings include recommendations in the use of capacitive methods aimed at determining equilibrium ion concentration.

SUPPLEMENTARY MATERIAL

See the supplementary material including numerical simulation input parameters and additional results.

ACKNOWLEDGMENTS

G.G.B. acknowledges the financial support from Generalitat Valenciana under Pla Complementari "Programa de Materials Avançats," 2022 (Grant No. MFA/2022/030). O.A. acknowledges funding from Departament de Recerca i Universitats, Departament d'Acció Climàtica, Alimentació i Agenda Rural i el Fons Climàtic de la Generalitat de Catalunya for the project Conversion of Energy in Sustainable Chemicals (CESC, Grant No. 2023 CLIMA 00067).

AUTHOR DECLARATIONS

Conflict of Interest

The authors have no conflicts to disclose.

Author Contributions

Germà Garcia-Belmonte: Conceptualization (equal); Data curation (equal); Formal analysis (equal); Funding acquisition (equal); Supervision (equal); Validation (equal); Visualization (equal); Writing – original draft (equal); Writing – review & editing (equal). **Osbel Almora**: Conceptualization (equal); Data curation (equal); Formal analysis (equal); Funding acquisition (equal); Supervision (equal); Validation (equal); Visualization (equal); Writing – original draft (equal); Writing – review & editing (equal).

DATA AVAILABILITY

The data that support the findings of this study are openly available in Github, at https://github.com/barnesgroupICL/Driftfusion, reference number JCEL2022.

REFERENCES

[1] A. Dualeh, T. Moehl, N. Tétreault, J. Teuscher, P. Gao, M. K. Nazeeruddin, and M. Grätzel, ACS Nano **8**(1), 362 (2014).
[2] H. J. Snaith, A. Abate, J. M. Ball, G. E. Eperon, T. Leijtens, N. K. Noel, S. D. Stranks, J. T.-W. Wang, K. Wojciechowski, and W. Zhang, J. Phys. Chem. Lett. **5**(9), 1511 (2014); H.-S. Kim and N.-G. Park, J. Phys. Chem. Lett. **5**(17), 2927 (2014).
[3] T. Eisenbarth, R. Caballero, M. Nichterwitz, C. A. Kaufmann, H.-W. Schock, and T. Unold, J. Appl. Phys. **110**(9) (2011).
[4] R. S. Sanchez, V. Gonzalez-Pedro, J.-W. Lee, N.-G. Park, Y. S. Kang, I. Mora-Sero, and J. Bisquert, J. Phys. Chem. Lett. **5**(13), 2357 (2014); E. J. Juarez-Perez, R. S. Sanchez, L. Badia, G. Garcia-Belmonte, Y. S. Kang, I. Mora-Sero, and J. Bisquert, J. Phys. Chem. Lett. **5**(13), 2390 (2014); J. M. Frost, K. T. Butler, and A. Walsh, APL Mater. **2**(8), 081506 (2014); J. Wei, Y. Zhao, H. Li, G. Li, J. Pan, D. Xu, Q. Zhao, and D. Yu, J. Phys. Chem. Lett. **5**(21), 3937 (2014).
[5] E. L. Unger, E. T. Hoke, C. D. Bailie, W. H. Nguyen, A. R. Bowring, T. Heumüller, M. G. Christoforo, and M. D. McGehee, Energy Environ. Sci. **7**(11), 3690 (2014).
[6] H.-W. Chen, N. Sakai, M. Ikegami, and T. Miyasaka, J. Phys. Chem. Lett. **6**(1), 164 (2015).
[7] Y. Shao, Z. Xiao, C. Bi, Y. Yuan, and J. Huang, Nat. Commun. **5**(1), 5784 (2014).
[8] Z. Xiao, Y. Yuan, Y. Shao, Q. Wang, Q. Dong, C. Bi, P. Sharma, A. Gruverman, and J. Huang, Nat. Mater. **14**(2), 193 (2015).
[9] H. Iwahara, Solid State Ionics **52**(1–3), 99 (1992).
[10] O. Almora, I. Zarazua, E. Mas-Marza, I. Mora-Sero, J. Bisquert, and G. Garcia-Belmonte, J. Phys. Chem. Lett. **6**(9), 1645 (2015).
[11] E. Hernández-Balaguera, B. Arredondo, G. d. Pozo, and B. Romero, Commun. Nonlinear Sci. Numer. Simul. **90**, 105371 (2020).
[12] E. Hernández-Balaguera, B. Romero, M. Najafi, and Y. Galagan, Adv. Mater. Interfaces **9**(9), 2102275 (2022); W. Choi, S. W. Song, S. G. Han, and K. Cho, Adv. Electron. Mater. **6**(6), 2000030 (2020); I. Zarazua, G. Han, P. P. Boix, S. Mhaisalkar, F. Fabregat-Santiago, I. Mora-Seró, J. Bisquert, and G. Garcia-Belmonte, J. Phys. Chem. Lett. **7**(24), 5105 (2016); I. Zarazua, J. Bisquert, and G. Garcia-Belmonte, *ibid.* **7**(3), 525 (2016).
[13] D. A. Jacobs, H. Shen, F. Pfeffer, J. Peng, T. P. White, F. J. Beck, and K. R. Catchpole, J. Appl. Phys. **124**(22), 225702 (2018); A. Schiller, S. Jenatsch, B. Blülle, M.

A. Torre Cachafeiro, F. Ebadi, N. Kabir, M. Othman, C. M. Wolff, A. Hessler-Wyser, C. Ballif, W. Tress, and B. Ruhstaller, J. Phys. Chem. Lett. **15**(45), 11252 (2024).
[14]Y. Yuan, J. Chae, Y. Shao, Q. Wang, Z. Xiao, A. Centrone, and J. Huang, Adv. Energy Mater. **5**(15), 1500615 (2015).
[15]S. A. L. Weber, I. M. Hermes, S.-H. Turren-Cruz, C. Gort, V. W. Bergmann, L. Gilson, A. Hagfeldt, M. Graetzel, W. Tress, and R. Berger, Energy Environ. Sci. **11**(9), 2404 (2018).
[16]H. Wang, Y. Bao, J. Li, D. Li, M. An, L. Tang, J. Li, H. Tang, Y. Chi, J. Xu, and Y. Yang, J. Phys. Chem. Lett. **14**(44), 9943 (2023).
[17]Y. Liu, L. A. Renna, H. B. Thompson, Z. A. Page, T. Emrick, M. D. Barnes, M. Bag, D. Venkataraman, and T. P. Russell, Adv. Energy Mater. **7**(21), 1701235 (2017).
[18]D. Moia, I. Gelmetti, P. Calado, Y. Hu, X. Li, P. Docampo, J. de Mello, J. Maier, J. Nelson, and P. R. F. Barnes, Phys. Rev. Appl. **18**(4), 044056 (2022).
[19]J. Thiesbrummel, S. Shah, E. Gutierrez-Partida, F. Zu, F. Peña-Camargo, S. Zeiske, J. Diekmann, F. Ye, K. P. Peters, K. O. Brinkmann, P. Caprioglio, A. Dasgupta, S. Seo, F. A. Adeleye, J. Warby, Q. Jeangros, F. Lang, S. Zhang, S. Albrecht, T. Riedl, A. Armin, D. Neher, N. Koch, Y. Wu, V. M. Le Corre, H. Snaith, and M. Stolterfoht, Nat. Energy **9**(6), 664 (2024).
[20]A. O. Alvarez, F. Lédée, M. García-Batlle, P. López-Varo, E. Gros-Daillon, J. M. Guillén, J.-M. Verilhac, T. Lemercier, J. Zaccaro, L. F. Marsal, G. Garcia-Belmonte, and O. Almora, ACS Phys. Chem. Au **3**, 386 (2023).
[21]G. Y. Kim, A. Senocrate, D. Moia, and J. Maier, Adv. Funct. Mater. **30**(31), 2002426 (2020).
[22]N. S. Hill, M. V. Cowley, N. Gluck, M. H. Fsadni, W. Clarke, Y. Hu, M. J. Wolf, N. Healy, M. Freitag, T. J. Penfold, G. Richardson, A. B. Walker, P. J. Cameron, and P. Docampo, Adv. Mater. **35**(32), 2302146 (2023).
[23]A. Guerrero, J. Bisquert, and G. Garcia-Belmonte, Chem. Rev. **121**(23), 14430 (2021).
[24]J. Diekmann, F. Peña-Camargo, N. Tokmoldin, J. Thiesbrummel, J. Warby, E. Gutierrez-Partida, S. Shah, D. Neher, and M. Stolterfoht, J. Phys. Chem. Lett. **14**(18), 4200 (2023).
[25]O. Almora, A. Guerrero, and G. Garcia-Belmonte, Appl. Phys. Lett. **108**(4), 043903 (2016).
[26]J. Caram, M. García-Batlle, O. Almora, R. D. Arce, A. Guerrero, and G. Garcia-Belmonte, Appl. Phys. Lett. **116**(18), 183503 (2020).
[27]P. Calado, I. Gelmetti, B. Hilton, M. Azzouzi, J. Nelson, and P. R. F. Barnes, J. Comput. Electron. **21**, 960 (2022).
[28]L. Bertoluzzi, J. B. Patel, K. A. Bush, C. C. Boyd, R. A. Kerner, B. C. O'Regan, and M. D. McGehee, Adv. Energy Mater. **11**(10), 2002614 (2021); B. Olyaeefar, S. Ahmadi-Kandjani, and A. Asgari, Physica E **94**, 118 (2017).
[29]O. Almora, D. Miravet, I. Gelmetti, and G. Garcia-Belmonte, Phys. Status Solidi RRL **16**(12), 202200336 (2022).
[30]A. O. Alvarez, M. García-Batlle, F. Lédée, E. Gros-Daillon, J. M. Guillén, J.-M. Verilhac, T. Lemercier, J. Zaccaro, L. F. Marsal, O. Almora, and G. Garcia-Belmonte, Adv. Electron. Mater. **10**(11), 2400241 (2024).
[31]G. Richardson, S. E. J. O'Kane, R. G. Niemann, T. A. Peltola, J. M. Foster, P. J. Cameron, and A. B. Walker, Energy Environ. Sci. **9**(4), 1476 (2016).
[32]M. Diethelm, T. Lukas, J. Smith, A. Dasgupta, P. Caprioglio, M. Futscher, R. Hany, and H. J. Snaith, Energy Environ. Sci. **18**(3), 1385 (2025); T. Zhang, G. Yang, S. Wang, Y. Sui, Y. Zhao, Y. Huang, Z. Zheng, Z. Tang, X. Chen, and Y. Zhang, IEEE Electron Device Lett. **45**(12), 2459 (2024).
[33]V. S. Bagotsky, *Fundamentals of Electrochemistry* (Wiley, Hoboken, 2005), p. 705.
[34]S. P. Mitoff and R. J. Charles, J. Appl. Phys. **43**(3), 927 (1972).
[35]A. Pitarch, J. Bisquert, and G. Garcia-Belmonte, J. Non-Cryst. Solids **324**(1–2), 196 (2003).
[36]O. Almora, C. Aranda, E. Mas-Marzá, and G. Garcia-Belmonte, Appl. Phys. Lett. **109**(17) (2016).
[37]S. M. Sze, Y. Li, and K. K. NG, *Physics of Semiconductor Devices* (Wiley, Hoboken, 2021), p. 203.
[38]M. García-Batlle, S. Deumel, J. E. Huerdler, S. F. Tedde, O. Almora, and G. Garcia-Belmonte, Adv. Photonics Res. **3**, 2200136 (2022).
[39]L. McGovern, M. H. Futscher, L. A. Muscarella, and B. Ehrler, J. Phys. Chem. Lett. **11**(17), 7127 (2020).
[40]L. Bertoluzzi, C. C. Boyd, N. Rolston, J. Xu, R. Prasanna, B. C. O'Regan, and M. D. McGehee, Joule **4**(1), 109 (2020); S. Reichert, Q. An, Y.-W. Woo, A. Walsh, Y. Vaynzof, and C. Deibel, Nat. Commun. **11**(1), 6098 (2020).
[41]O. Almora, Ph.D. thesis, Friedrich-Alexander Universität Erlangen-Nürnberg & Universitat Jaume I, 2020.
[42]M. Fischer, K. Tvingstedt, A. Baumann, and V. Dyakonov, ACS Appl. Energy Mater. **1**(10), 5129 (2018).
[43]K. Zhang, A. Späth, O. Almora, V. M. Le Corre, J. Wortmann, J. Zhang, Z. Xie, A. Barabash, M. S. Hammer, T. Heumüller, J. Min, R. Fink, L. Lüer, N. Li, and C. J. Brabec, ACS Energy Lett. **7**(10), 3235 (2022); E. Ghahremanirad, O. Almora, S. Suresh, A. A. Drew, T. H. Chowdhury, and A. R. Uhl, Adv. Energy Mater. **13**(30), 2204370 (2023).